USING UAV'S IMAGERY VEGETATION INDICES COMBINATION IN DELINEATION OF SOIL MAP UNITS

Layla A. Abdelelah **Kusay A. Wheib**
Researcher **Assist. Prof.**
Dept. of Soil Sciences and Water Resources, Coll. of Agric. Engin. Sci., University of Baghdad
Kusay.wheib@coagri.uobaghdad.edu.iq

ABSTACT

Alsweira research farm (44.823410 and 44.823040 N, 33.012701 and 33.012090 E) of an area of 5000 Da., was selected to conduct the UAV's photogrammetry interpretation to delineate and separate soil units at the series level in collaboration with the measured RGB vegetation indices derived from their data. Visual interpretation of mosaic and the vegetation indices efficiently eased the delineation process of soil series map. RGB indices measured form UAV's imagery were efficient in delineating soil units, and they showed significant relationships with above ground biomass where the later is representing the vegetation cover in the study area. NGRDI, ExG, NExG, and RGBVI showed high correlation with above ground biomass (g m^{-2}) while VARI showed no relationship with it. Percentages of Indices participation in delineation and isolation of map units were as follow: NGRDI> RGBVI > NexG> ExG> VARI in 90%, 89%, 86%, 85%, and 52% respectively.

Keywords: UAV's, Drones, vegetation indices, NGRDI, ExG, NExG, RGBVI, VARI
***Part of the M.Sc. thesis of the 1st author.**

مجلة العلوم الزراعية العراقية- 2025 :56 (عدد خاص):132-147 **عبدالاله و هيب**

ليلى احمد عبد الاله **قصي عبد الرزاق وهيب**
باحث **أستاذ مساعد**
قسم علوم التربة والموارد المائية، كلية علوم الهندسة الزراعية، جامعة بغداد

المستخلص

تم اختيار مزرعة الصويرة البحثية (بين خطي طول 44.823410 و 44.823040 شمالا ودائرتي عرض 33.012701 و 33.012090 شرقا) لإجراء تفسير التصوير المساحي للطائرة بدون طيار لتحديد وفصل وحدات التربة على مستوى السلسلة بالاستعانة بأدلة الغطاء النباتي المحسوبة من انعكاسيات الاطوال الموجية المرئية RGB للصور الملتقطة لمنطقة الدراسة. أدى التفسير المرئي للموزائيك ومؤشرات الغطاء النباتي إلى تسهيل عملية ترسيم خريطة سلسلة التربة بكفاءة. كانت الأدلة الخضرية المحسوبة من الاطوال الموجية المرئية RGB المقاسة من صور الطائرات بدون طيار فعالة في تحديد وحدات التربة، وأظهرت علاقات مهمة مع الكتلة الحيوية فوق الأرض حيث يمثل الأخير الغطاء النباتي في منطقة الدراسة. أظهرت الأدلة الخضرية NGRDI وExG وNExG وRGBVI ارتباطًا عاليًا بالكتلة الحيوية فوق الأرض (غم م $^{-2}$) بينما لم يظهر VARI أي علاقة بها. وكانت النسب المئوية لمشاركة المؤشرات في ترسيم وعزل وحدات الخريطة على النحو التالي: NGRDI> RGBVI> NexG> ExG> VARI بنسبة 90%، 89%، 86%، 85%، و52% على التوالي.

كلمات مفتاحية: المركبات بدون طيار، درونز، الأدلة الخضرية، NGRDI, ExG, NExG, RGBVI, VARI
***البحث جزء من رسالة ماجستير للباحث الأول.**

Received:17/3/2024, Accepted:23/6/2024

INTRODUCTION

Specific area on the map that has physical and chemical properties that differ from another area is called map unit (3,18). Soil units can be mapped as a photomorphic units where maps are a miniature drawing of a specific area on the surface of the ground (1, 7). There are different types of maps. The most important types of maps used in the agricultural field are soil classification and salinity maps (24). Map units are considered the basic language of geographical sciences and other sciences, including agriculture (4, 9). Soil units are classified according to the components of the soil, its shape and size, according to the study or the intended goal (8). The basic component of map units is the soil units. They may be classification units or units that make up groups of soil units (16). Soils can be distinguished and separated from each other in nature on the ground and maps (31). Maps are the most important means of visual spatial identification, through which a coordinate definition can be made of the phenomena present on the surface of the ground and their various types, including the concept of soil, the unity of maps of spatial and temporal variations, and their interpretation, including the relationship of soil with the terrestrial perspective (13, 15). Soil variability is considered as a challenge in mapping soil units especially in mapping soil properties (27). The development of technology, especially the use of drones in various fields such as health, the military field, and the field of agriculture. UAV's support many tasks such as surveying and transportation in agriculture (5, 19). The use of drones in the agricultural field is low-cost, and accurate information and measurements can be obtained compared to other devices (29). Hamad and Suliman (12) used aerial photographs captured by UAV's to separate map units at the soil series level, and the found that the most suitable altitude of the used drone to be at 100 m above ground, also, they confirmed that using drones' photographs in soil management, mapping, and agricultural field development. Reg, (22) has also confirmed that using UAV's photographs for the purposes of crop scan in the field to detect variation in growth stages and field management. Wheib et al., (28) used UAV's to monitor wheat crop variation throughout growth season using the vegetation indices derived from wavelength of aerial photography, and they confirmed that the Normalized green red difference index was good for their objectives. Al-Jubouri et al., (2) used aerial photograph as base maps to produce soil survey and classification maps at the series level in Sheikh Saad project in Iraq, and they confirmed that on the level of accuracy, UAV's photos were efficient and effective in mapping soil series. Wadod and Mohammed, (26) have done a review in using drones in precision agriculture, and they confirmed that farms are easier to manage using drones as an application to sustain production and increase crop yield. Also, Jasim et al., (14) had used active and passive sensors to predict phosphorus and potato yields, where those sensors are representing the aerial images generated by crop circle as active sensor and green seeker as passive sensors where they confirmed that the crop circle imagery was more representative to phosphorus uptake than green seeker. Objectives of this study is focusing on using aerial photographs captured by UAV's and RGB vegetation indices to delineate and separate soil units at the series level.

MATERIALS AND METHODS

Location: Alsweira Farm is located within the lands of Wasit Governorate, on the eastern bank of the Tigris River, about 50 km southeast of Baghdad. It is bordered to the north by the Nahrawan Canal, to the south by the Tigris River, to the east by the Hafriya Project, and to the west by the Salman Pak Project. The soil of the Alsweira Model Farm (Alsweira Research Station) was surveyed by the Directorate of Soil and Public Land Reclamation (abolished), with an area of five thousand dunums. Figure (1) represents the study area.

Aerial photographs: Aerial images were taken with airborne cameras on DJI PILOT MAVIC 2 Enterprise dual remote drones, 24 mm viewfinder and 1/2.3 inch 12 MP sensor and aerial data (images) were collected near from midday (between 11 a.m. and 1 p.m.) to ensure that changes in the sun's azimuth were minimal. Aerial photographs were taken at an altitude of 100 meters (12). The spatial

resolution of the aerial images was 0.5 * 0.5 metres, and the area covered by the aerial image taken by the drone is about 1.45 hectares, with a cross-sectional area of approximately 145 * 100 m^2. A survey path was taken for the drone to take aerial images (figure 2), to cover the area with a total of 206 aerial images. The images overlapped with each other as a result of the movement of the drone. The Mosaic images were collected using the ArcMap 10.8 software, after geo-correcting the aerial images by projecting them onto a satellite image taken on the same date. They were returned as a base map, in addition to the control points that were collected while taking the first aerial image to determine their location on the satellite image to begin the mosaic process. The images were collected in a large mosaic format and the study area (the typical Alsweira farm) was cropped on a shapefile. The cropped aerial image was corrected after removing the distortions resulting from overlapping as a result of the mosaic first, and the radiation distortions resulting from the difference in the movement of the sun when taking the aerial image. Figure (3) shows the final mosaic aerial image composed for the study area. The study area (Alsweira Research Station) was georeferenced using a sapefile that was prepared based on the base map obtained from the station.

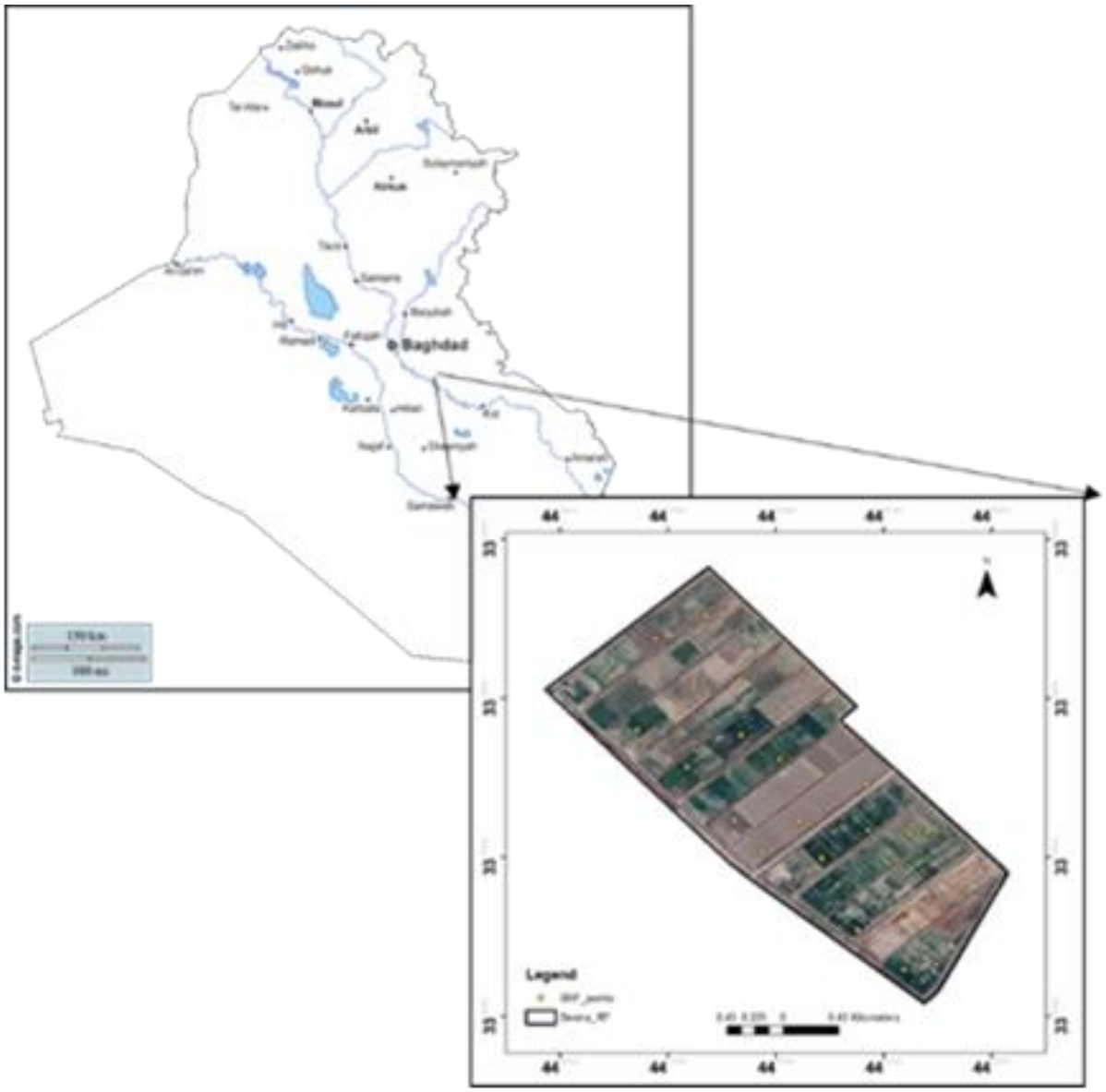

Figure 1. Map of Iraq showing Location of study area

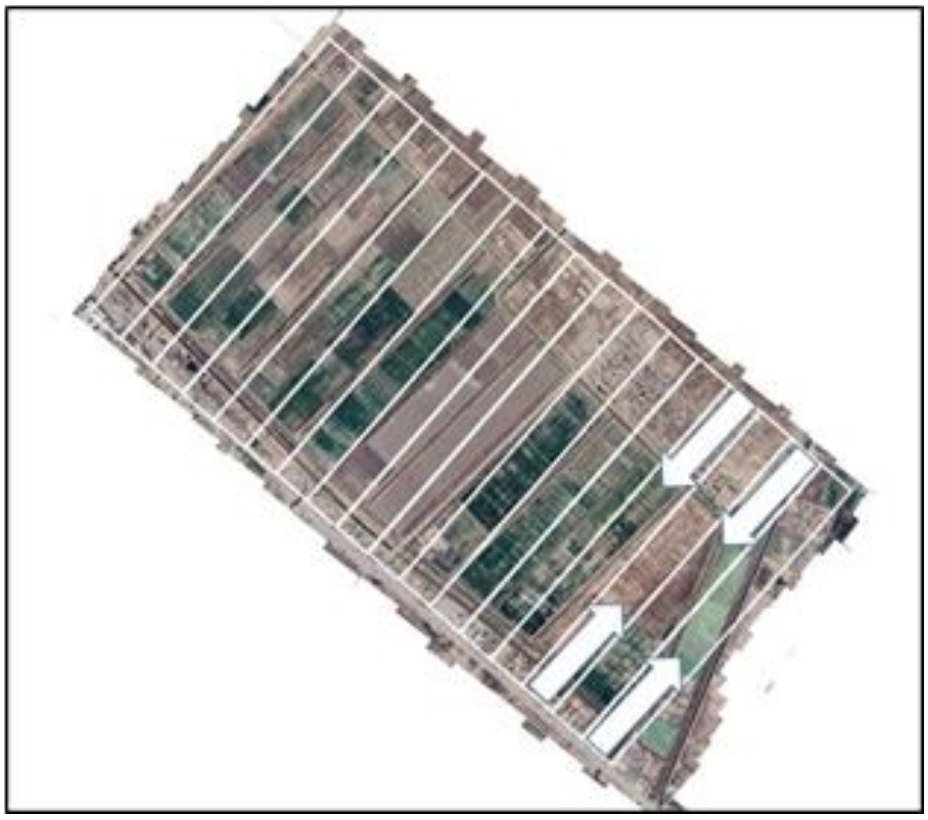

Figure 2. Aerial photos path movement and mosaic

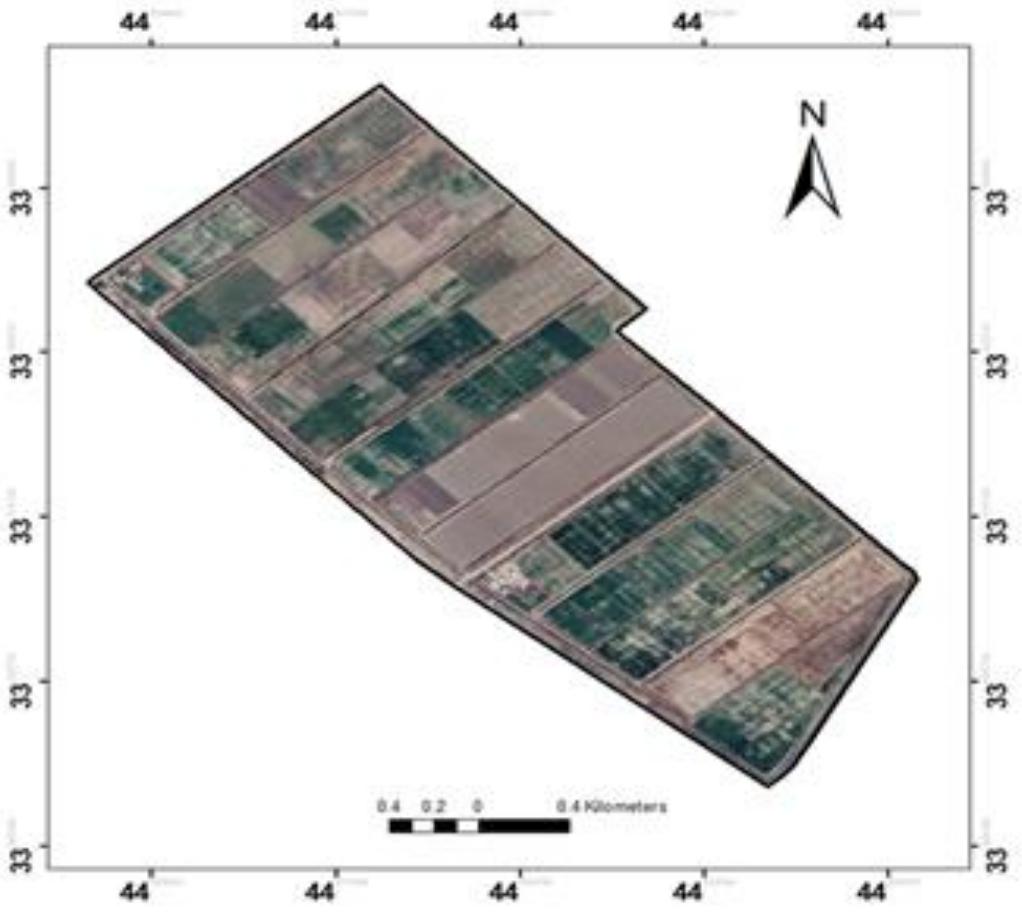

Figure 3. Final Aerial photos mosaic

Measured spectral Indices

1- NGRDI Normalized Green Red Difference Index

NGRDI= (Green –Red)/ (Green +Red)------(1) (25)

2- VARI Visible Atmospherically Resistant Index

VARI = (G – R) / (G + R – B)--- (2) (11)

3- Excess Green ExG Guide

ExG = 2GREEN − RED − BLUE -- (3) (30)

4- NExG Normalized Excess Green Guide

NExG = 2*GREEN – RED – BLUE/ GREEN + RED + BLUE --- (4) (30)

5- RGBVI Red Green Blue Vegetation Index

RGBVI = (Green*Green)– (Red*Blue)/(Green*Green)+(Red*Blue)--- (5) (6)

Sampling: Soil samples were collected after the visual interpretation of RGB indices besides the aerial photo interpretation.

RESULTS AND DISCUSSION

Field visits were conducted to explore the study area and obtain preliminary information such as a map of the location of the Alsweira Research Station, as well as revealing the soil formation factors in the study area such as the natural vegetation and the terrain raised in the area, as well as the land uses of the station's farm. A preliminary survey of the study area was conducted using auger holes to reveal the soil texture and depth of staining, and thus determine the soil chains spread in the study area using the free soil survey method. Which can be summed up by using all available formation factors in interpreting the spatial phenomena present in the study area, in addition to using available base maps or interpreting aerial photographs (20), where aerial photographs taken by UAV's were used to determine the paths of the sampling in integration with what was mentioned previously. After identifying the soil series from the examination points, the aerial photographs were used to isolate and separate the photographic units to complete the soil survey map. Figure (4) and table 1 show the percentages of dominance of soil series and classification details in the study area.

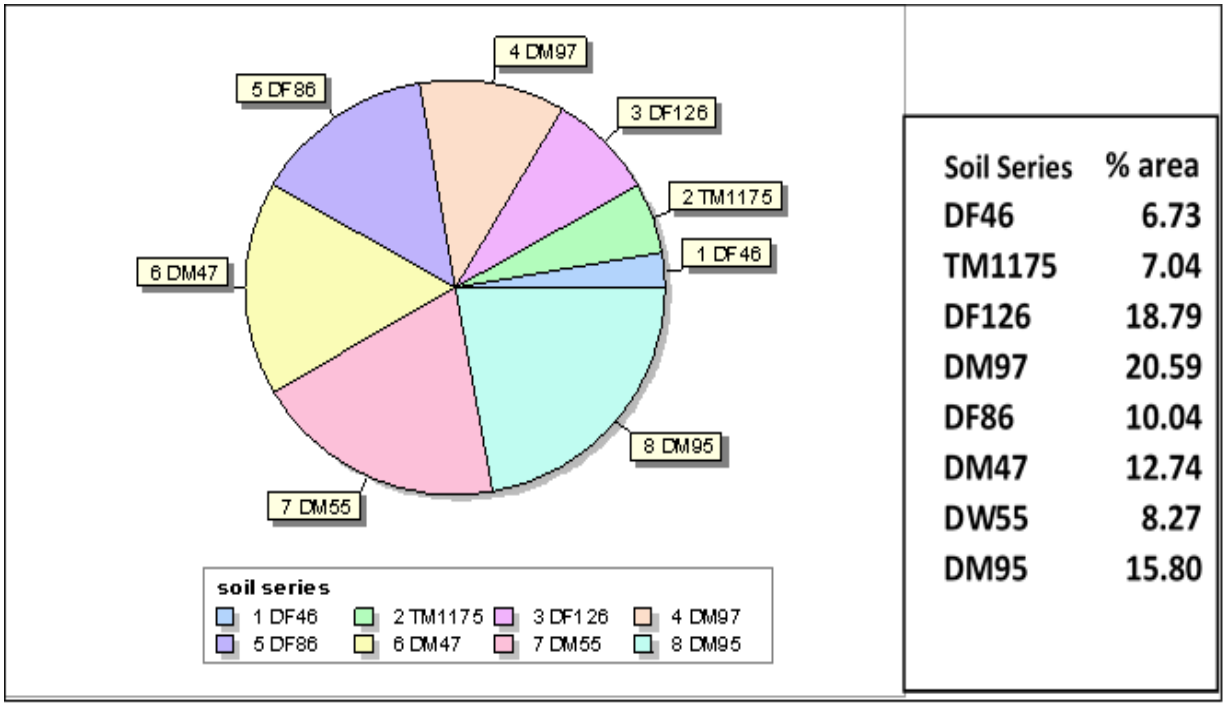

Soil Series	% area
DF46	6.73
TM1175	7.04
DF126	18.79
DM97	20.59
DF86	10.04
DM47	12.74
DW55	8.27
DM95	15.80

Figure 4. Percentages of dominance of soil series by area

Visual interpretation of the RGB indices measured prior to soil survey were used to delineate soil series, as figure (5) shows Soil Series map of Alsweira project area.

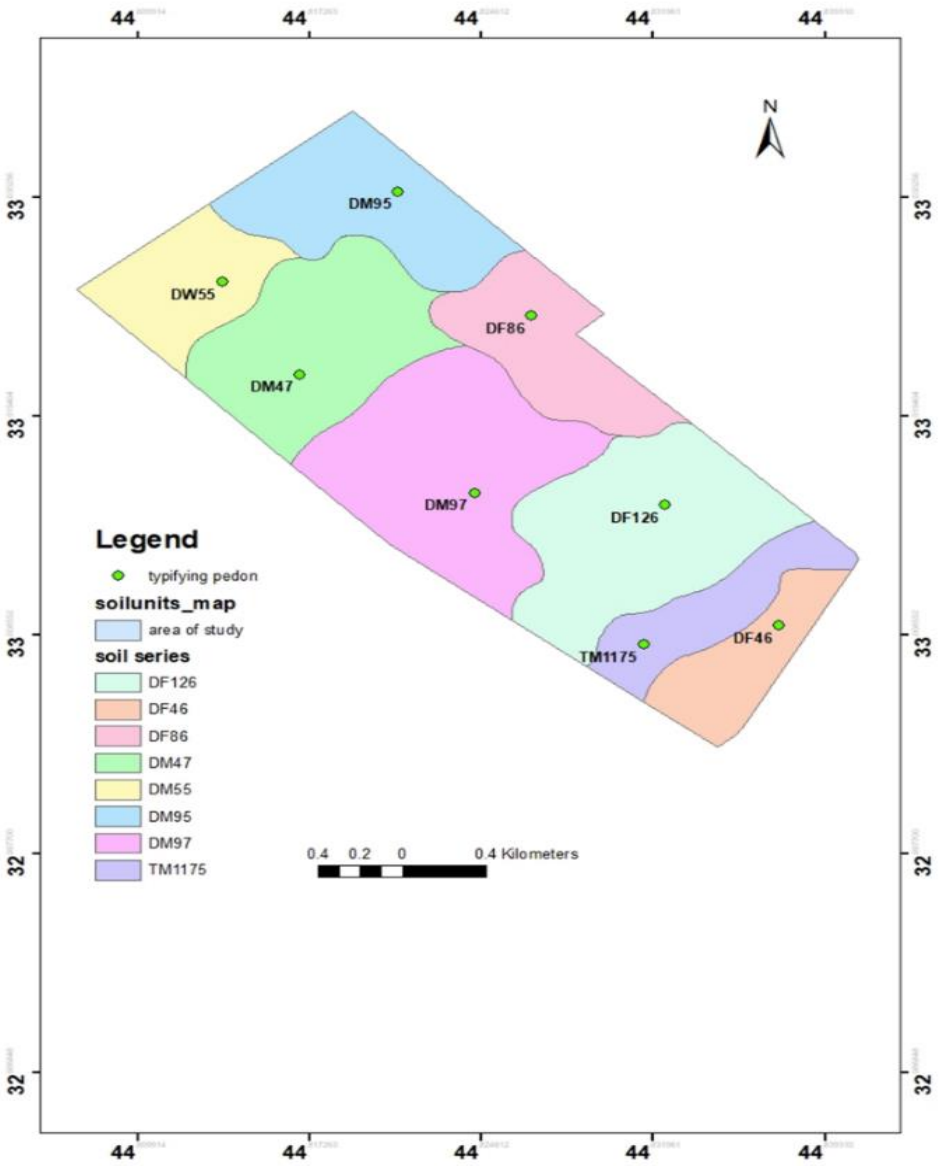

Figure 5. Soil series map of Alsweira project area

Table 1. Soil Series Units classification

Soil Series	Texture	Drainage	Classification stories
DF46	**L/SiCL**	**Imperfect**	**Di**
TM1175	**SiC/C/SiCL**	**Moderate**	**Tri**
DF126	**C/SiCL**	**Imperfect**	**Di**
DM97	**SiCL/SiC**	**Moderate**	**Di**
DM86	**CL/SiCL**	**Moderate**	**Di**
DM47	**L/SiCL**	**Moderate**	**Di**
DW55	**SiL/L**	**Well drain**	**Di**
DM95	**SiCL/SiL**	**Moderate**	**Di**

Above Ground Biomass (AGB)

The highest content of biomass above the soil surface reached 169.5 gm m-2 in the surface sample of the sixth pedon, which belongs to the soil series DW55, while its lowest content reached 7.31 gm m-2 in the third surface sample, which belongs to the soil series DF126. . Here it can be said that the intensity of land use affects the biomass content of the soil, but the matter is linked to the period of taking the sample. Lands prepared for agriculture may have a high content of organic carbon or total nitrogen, but it shows a decrease in the biomass content because the land is prepared for agriculture and may be devoid of plants. Sleeping in it at the time.

Also, soils affected by salts may be dominated by salt-tolerant plants with dense growth, as was observed during field visits and taking soil and plant samples compared to fields whose soil was prepared for cultivation. The coefficient of variance in above ground biomass reached up to 73%, which is relatively high. The reason here is due to the difference in the density of plants spread in the study area, whether natural or cultivated. It was noted that the fields cultivated with fodder crops were higher in their biomass content as well. In fact, it was observed that some abandoned lands with some natural plants growing had an increase in AGB compared to lands prepared for agriculture after the previously cultivated crop had been harvested, ploughed, and elevated, and thus almost devoid of plants. Figure (6) explains the above-ground biomass values distributed over the soil series in the study area. Figure (7) shows the spatial distribution of above-ground biomass distributed into four classes, in which the class 50-100 g m^{-2} dominated, followed by the class less than 50 g m^{-2} with a significant increase in soils with a biomass content of 100-150 g m^{-2}. It is worth noting that the increase in biomass values above the ground was spatially linked to land use, especially land cultivated with fodder crops, as in the DW55 and DM95 soil series, where those results were reflected by measured RGB indices.

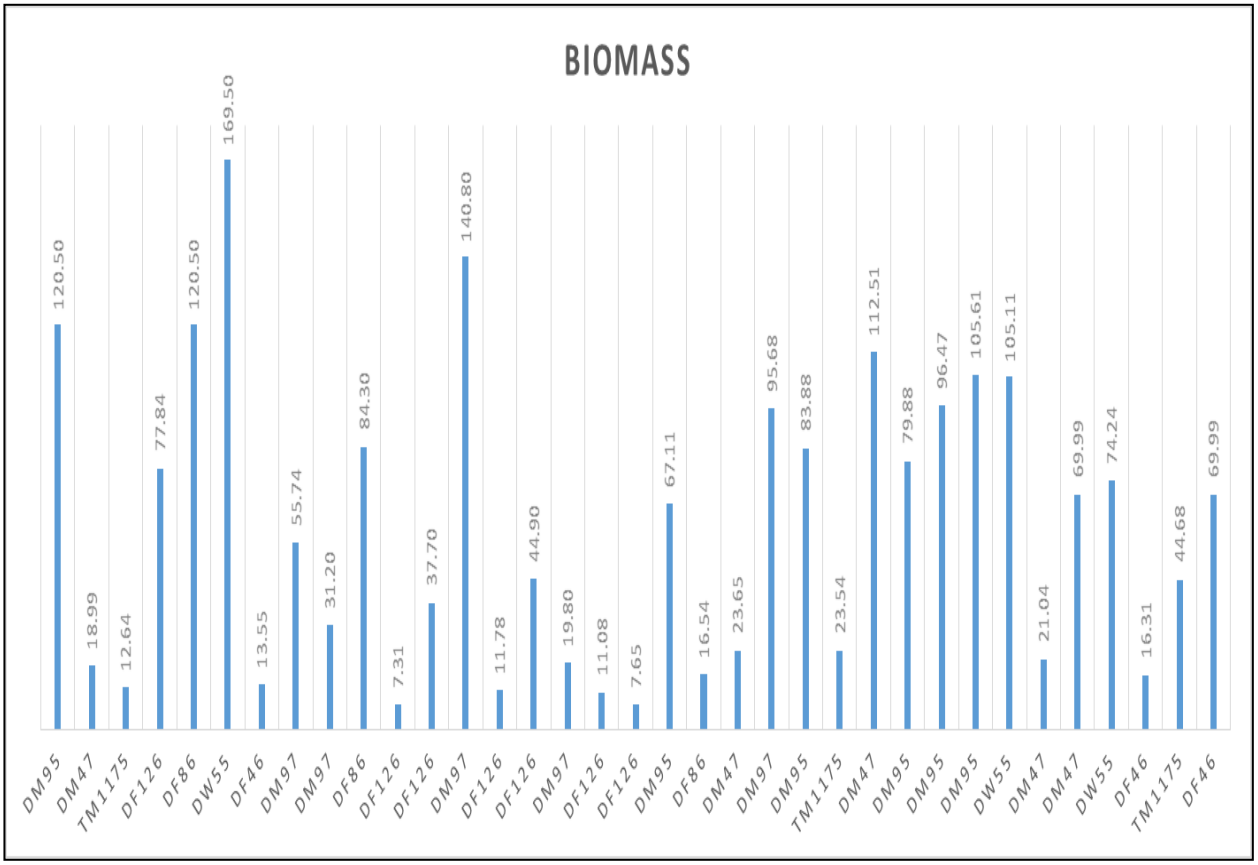

Figure 6. Biomass values in relation to soil series

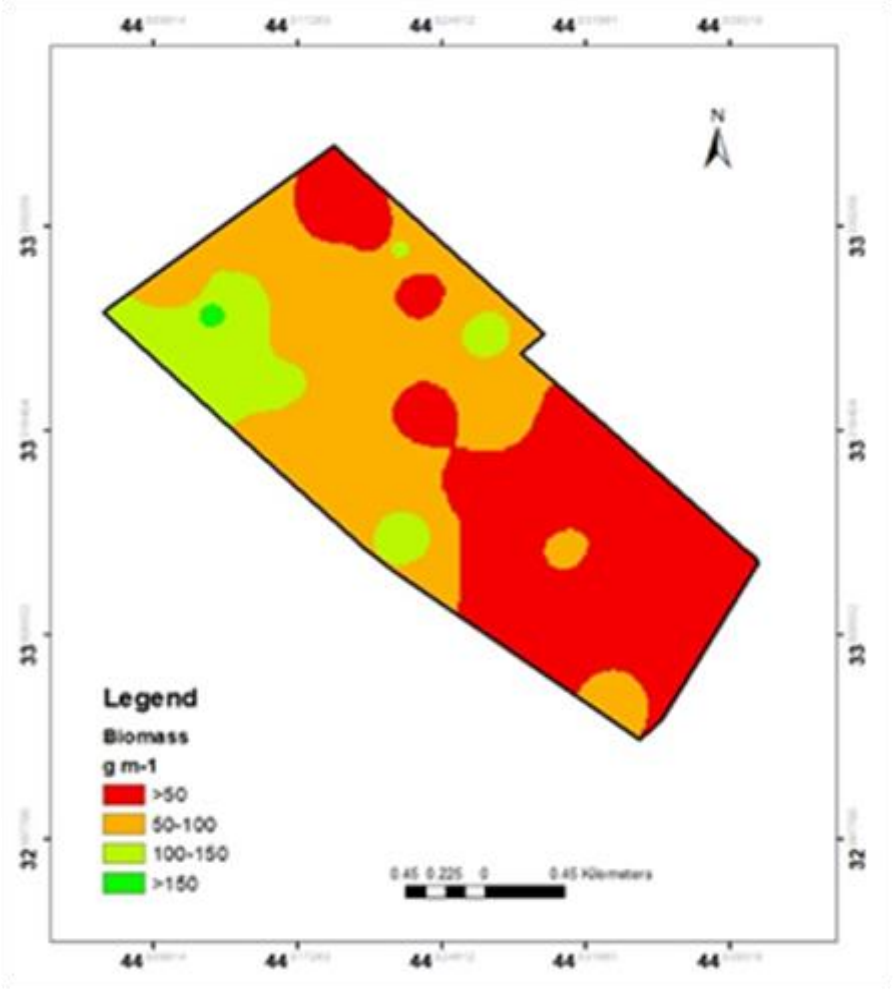

Figure 7. Spatial distribution of above ground biomass

Spectral Indices of UAV's photos

Normalized Green Red Difference Index NGRDI Figure (8) indicates a distribution map of the normalized red green cover difference index. This index indicates the difference between the reflectance of green and red modulated wavelengths. The greatest reflectance of vegetation at visible wavelengths, occurs at the green wavelength, while the lowest reflectance occurs at the red wavelength. Therefore, increasing the value of this index indicates an increase in the difference between the reflectance of green wavelengths and red ones, and whenever the value of this index increases, it indicates an increase in vegetation cover. Because this index is normalized, the values of this index range between (1 and -1), as the values of this index ranged in the same range in the study area. This index showed a clear, significant relationship (R^2= 0.66 $p<0.01$) with above-ground biomass, as the value of this index increases with increasing vegetation cover. Figure (9) shows that relationship. Soil series units were easier to delineate and separate using the lines of RGB indices here in addition to the aerial photointerpretation basics.

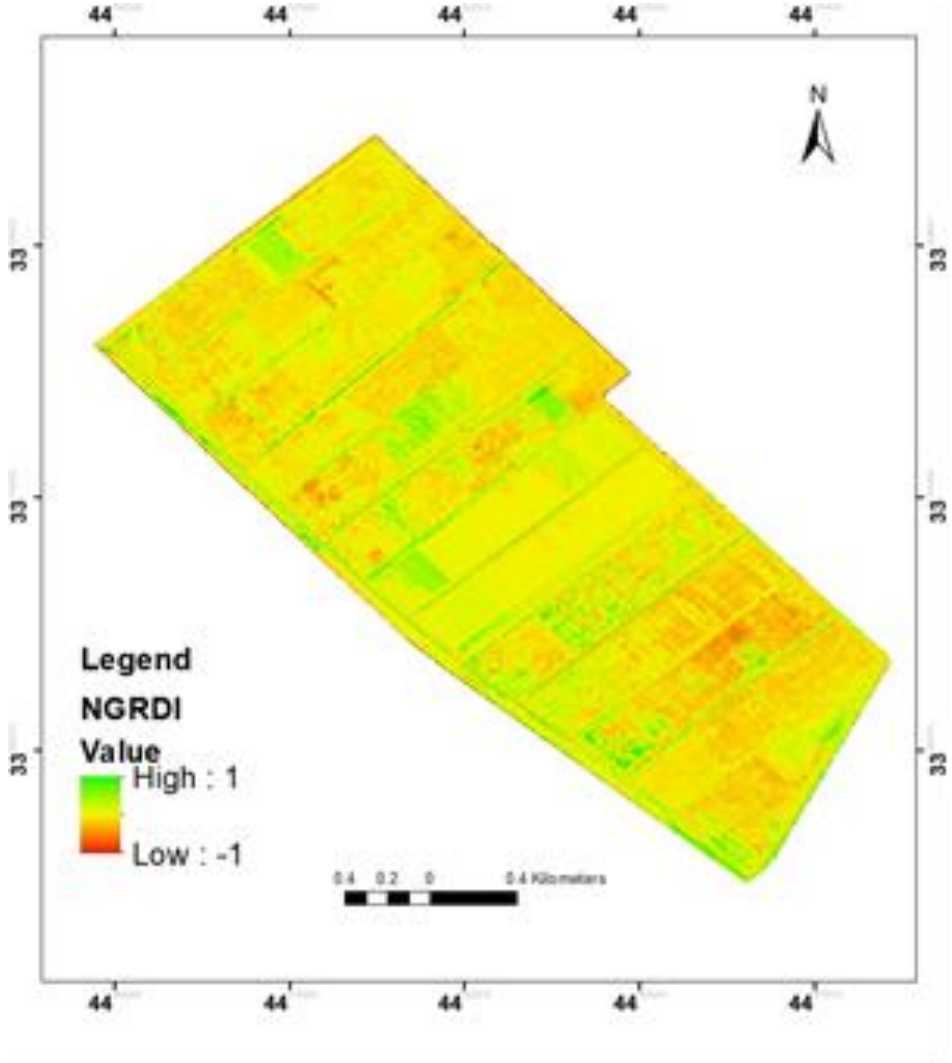

Figure 8. NGRDI distribution in Alsweira research f

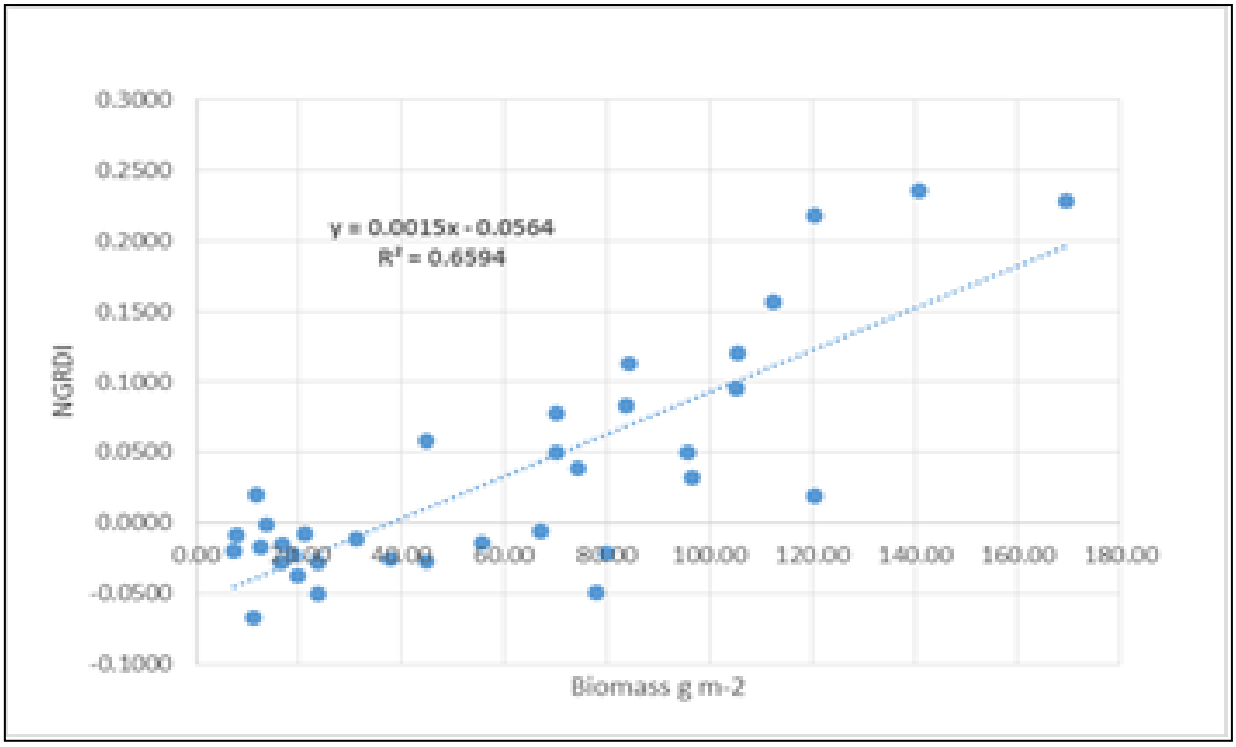

Figure 9. Relationship between NGRDI and biomass g m^{-2}

Excess Green Index (ExG)

Figure (10) indicates the spatial distribution map of the Excess Green Index calculated from the equation (3), which states that subtracting twice the reflectance of green wavelengths from red and blue. Therefore, the value of this index does not fall within a specific range, as it depends on the actual value of the reflectivity at each wavelength, where the values of this index in the study area ranged between 191 and -57, as with the increase of the value, the value of the index increases due to the increase in the green cover there. It is noted that this index was significantly associated with an increase in biomass per square meter in the study area (R^2 = 0.77 $p<0.01$). Figure (11) shows the relationship between this index and the above ground biomass, Zhou et al., 2023 confirmed that there is a high significance between biomass and this index besides other indices calculated from aerial photographs data captured by UAV's.

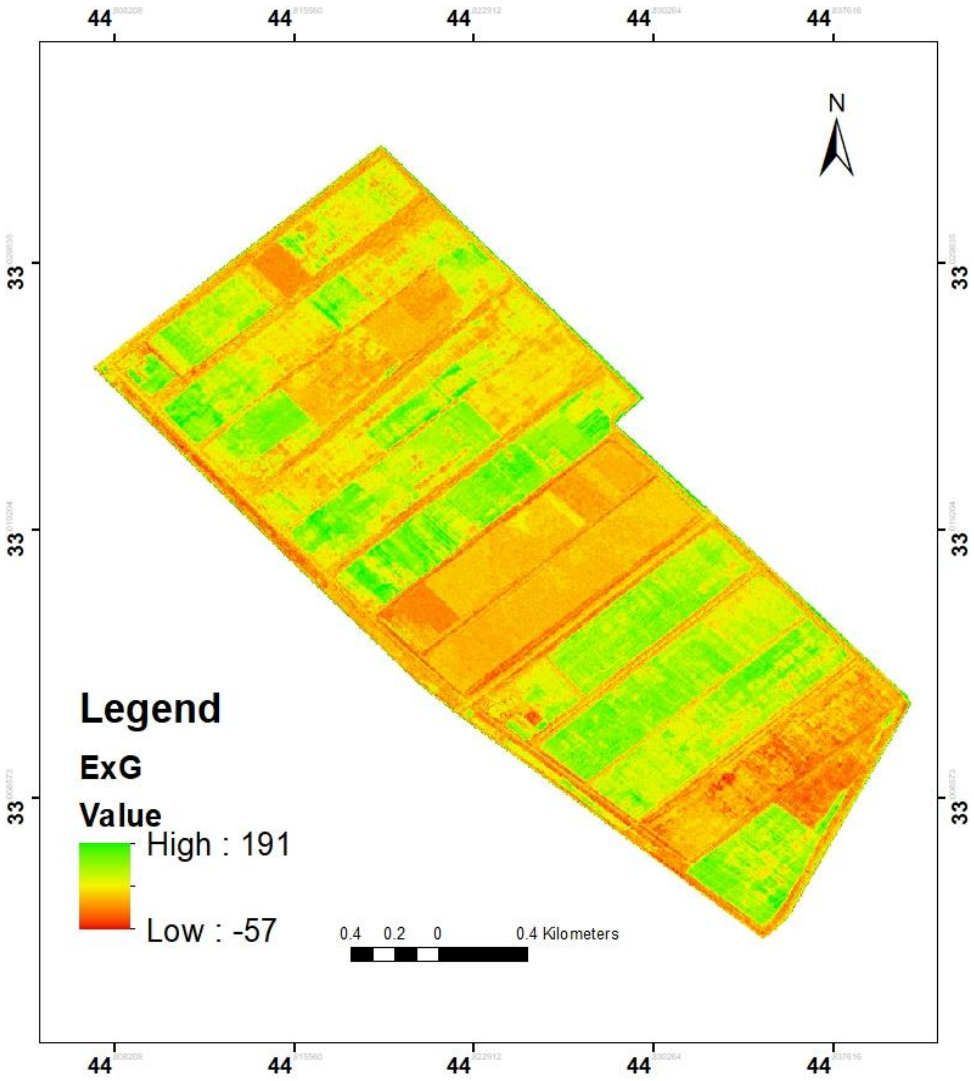

Figure 10. ExG distribution in Alsweira research farm

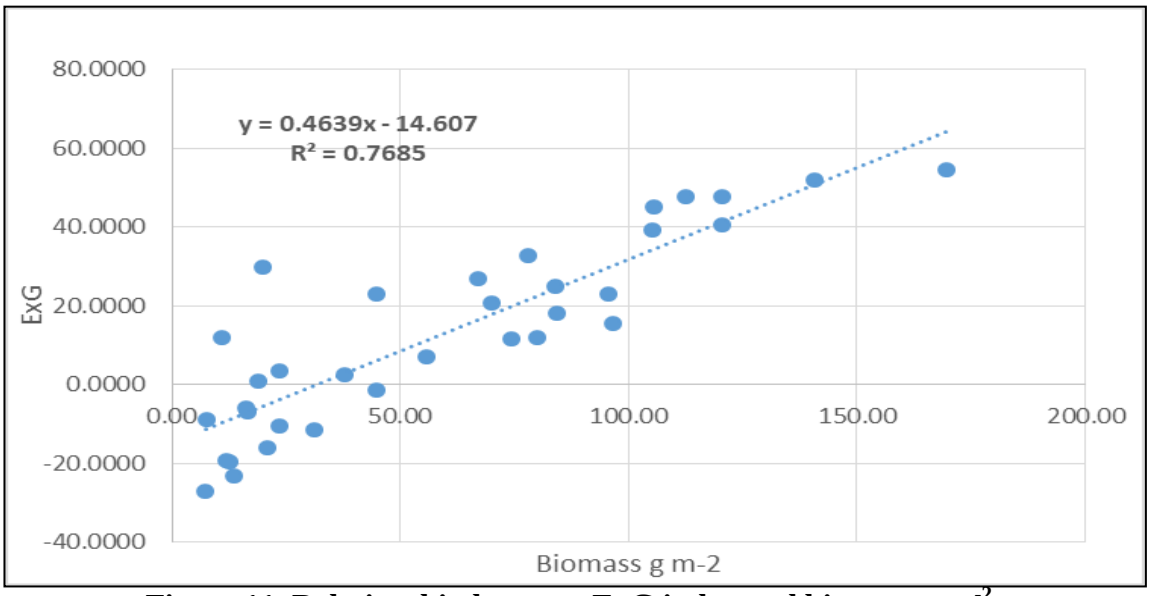

Figure 11. Relationship between ExG index and biomass g m^{-2}

Normalized Excess Green Index (NExG)

This index indicates twice the reflectance of the green spectrum (the most reflective of the plant leaf) subtracted from the red and blue spectrum (the most absorbent of the plant leaf) adjusted by dividing by the sum of the three visible spectra (equation 4). Therefore, the minimum possible value of this evidence is -1 and the highest is 2 (due to doubling the reflectance of the green spectrum multiplied by *2). Figure (12) indicates the spatial distribution map of the Normalized Excess Green Index. It is noted that higher values of this index were associated with cultivated soil series compared to abandon ones, as this feature was used to isolate soil series by determining separation delineations using spectral indices measured from aerial photographs data captured by UAV's. Figure (13) indicates the significant statistical relationship between the NExG index and the above ground biomass (g m^{-2}). The correlation coefficient reached 0.71 ($p< 0.01$). This indicates that an increase in biomass means an increase in vegetative growth, and therefore the NExG index is affected by vegetative cover.

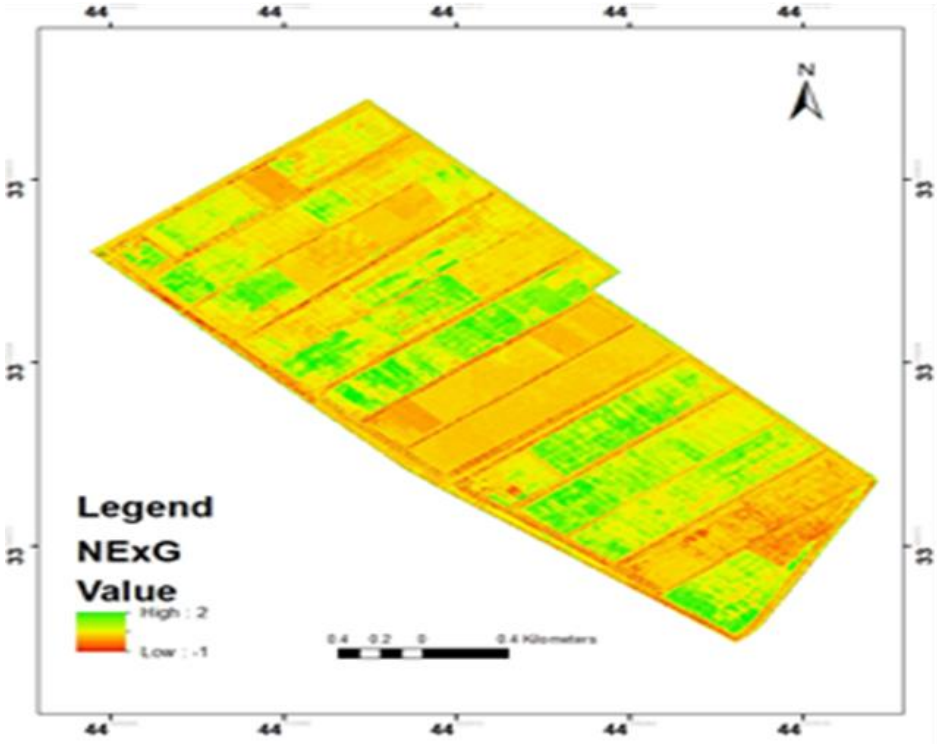

Figure 12. NExG distribution in Alsweira research farm

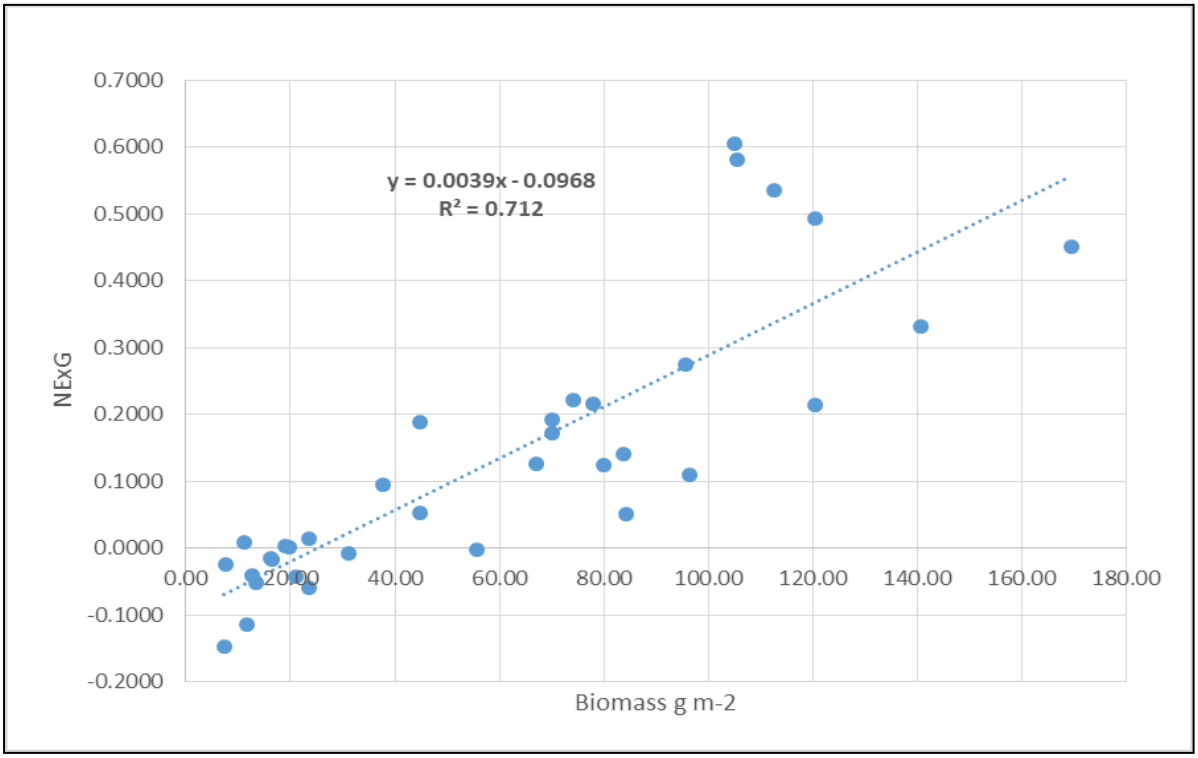

Figure 13. Relationship between NExG index and biomass g m^{-2}

Visible Atmospherically Resistant Index (VARI): Figure (14) indicates the spatial distribution of the green-to-red ratio index, (equation 2). When studying the statistical relationships (regression) between the characteristics of the vegetation cover (biomass), this index did not show a clear statistical relationship, even though it was an inverse relationship, and this was also confirmed by Prabhakara et al., (21).

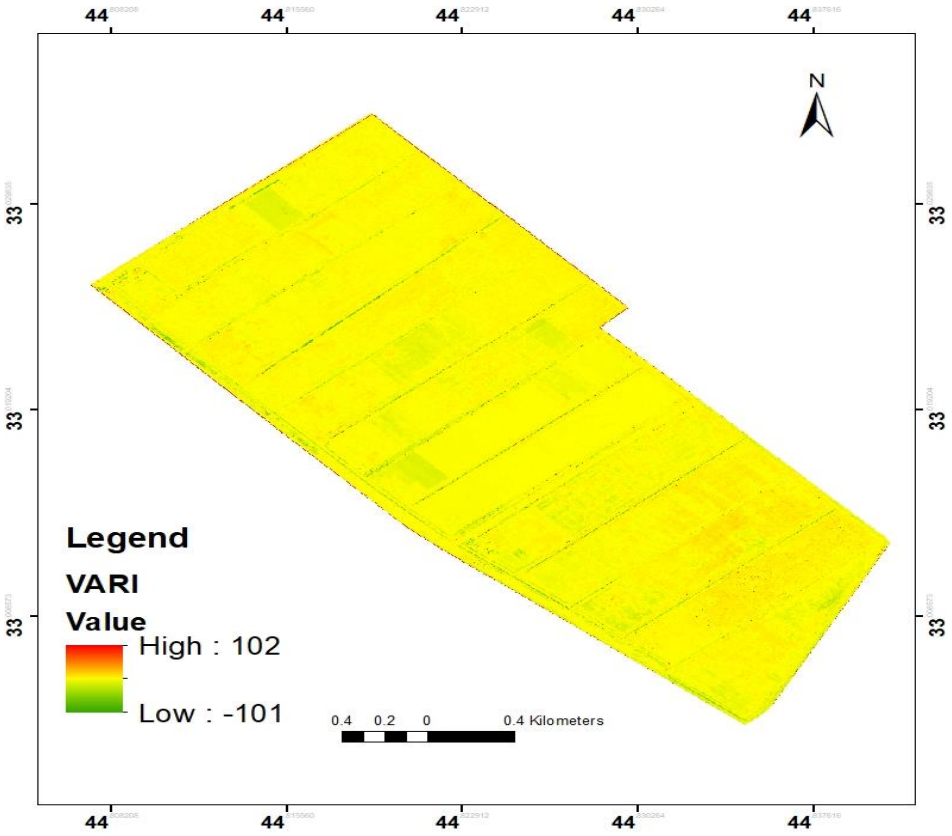

Figure 14. VARI distribution in Alsweira research farm

Red Green Blue Vegetation Index RGBVI This index is calculated from twice the green wavelength (the most reflectance) subtracted from the red and blue wavelengths (the least reflectance) divided by the sum of these spectra (equation 5). In other terms, it can be said that it is a normalized rate, so the range of this evidence ranges between 1 and -1. Figure (15) indicates a spatial distribution map of RGBVI index in the study area. The distribution of this index showed that most of the values were below zero (the locations of the study samples), but the high numbers that were close to 1 occurred in different locations. The reason may be due to doubling the green wavelength subtracted from the blue and red in the denominator of the equation. It is also worth noting that the value of this index was correlated to the spatial distribution of the soil series when visually interpreted, this index was significantly correlated to the distribution of biomass, (R^2 = 0.53, p <0.01) and Figure 16 shows this relationship. This was also confirmed by Liang et al., (17), Roth and Streit, (23).

Delineation of soil units (series) using vegetative evidence: After matching the map of the soil series prepared with eight soil units, they were matched with the maps of vegetative evidence to obtain the result of the contribution of each index to delineate and separate the photomorphic units visually and digitally. In more detail, this correspondence was calculated by change detection method between the soil series map and the vegetation indices as well, as the vegetative indices was classified into eight units to be similar to the soil chain units, as any increase or decrease when subtracting the first (soil chain map) from Which of the vegetative evidence gave a certain number of counts, and thus the sum of the differences was subtracted from the net total and converted into a percentage to represent the percentage of each evidence's contribution to the process of isolating and separating the soil units. Therefore, the percentage of contribution to separating and isolating the formal units was as follows:

NGRDI	RGBVI	NexG	ExG	VARI
90%	89%	86%	85%	52%

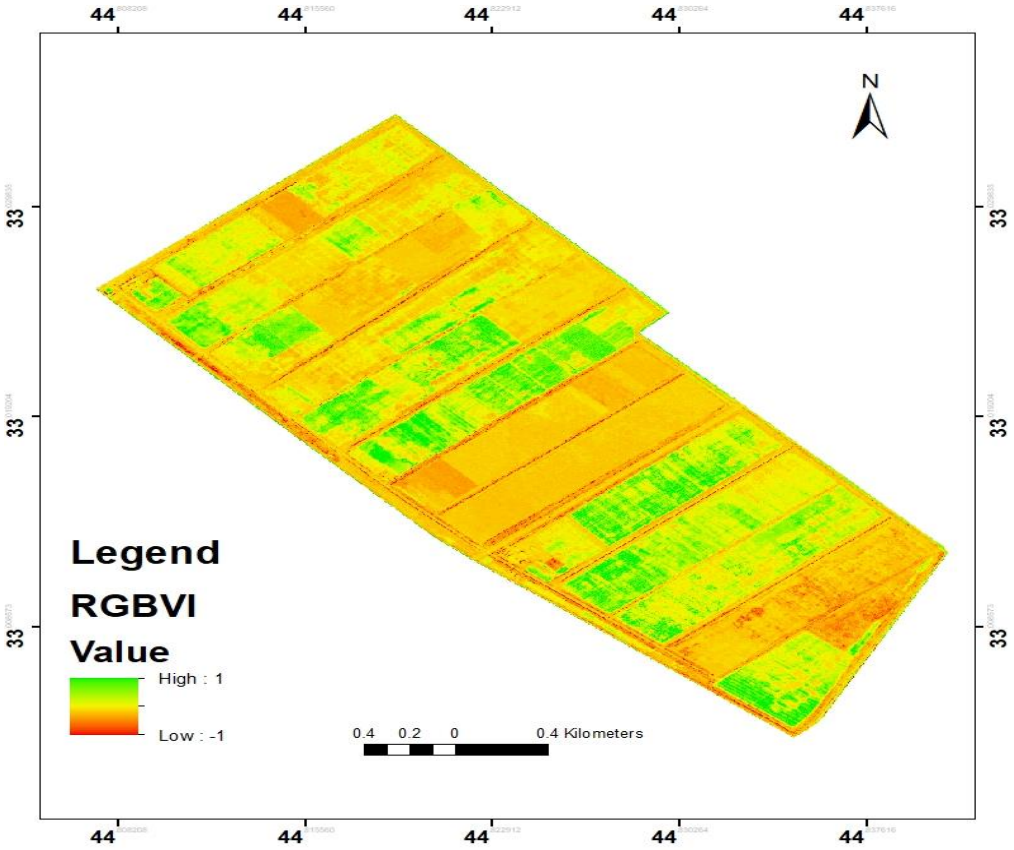

Figure 15. RGBVI distribution in Alsweira research farm

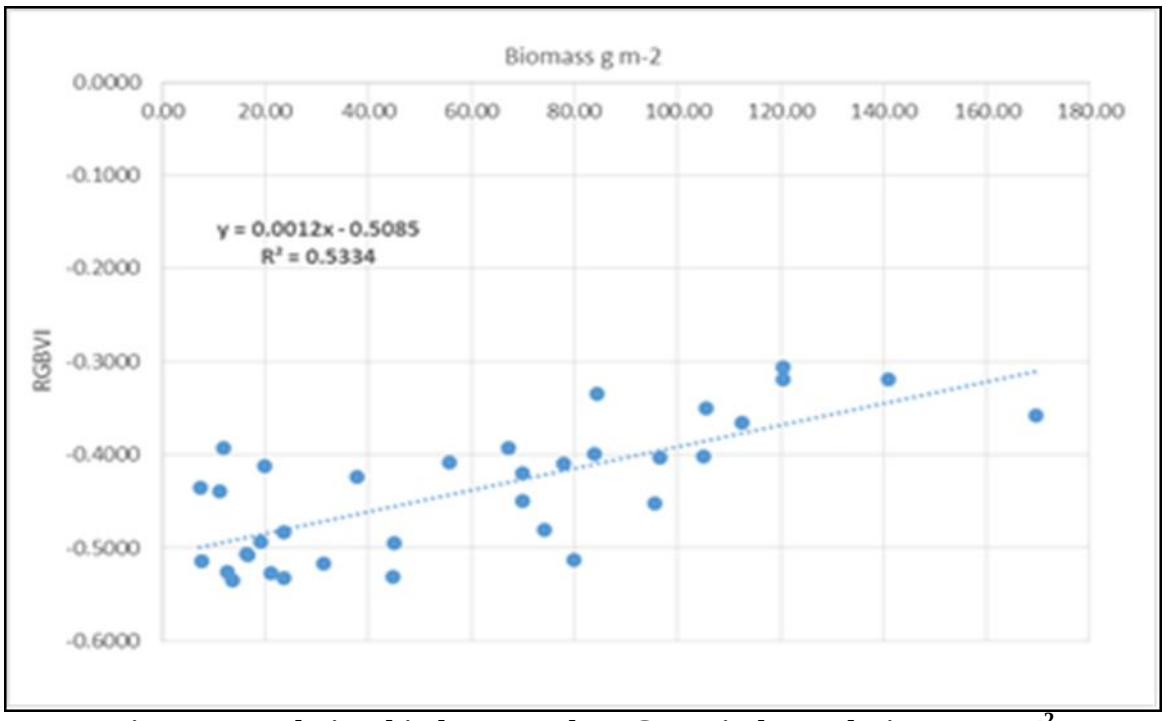

Figure 15. Relationship between the RGBVI index and Biomass g m^{-2}

REFERENCES

1. Abbass, J. A., and K. A. Wheib. 2007 Using Index of Compaction in interpreting the distribution and shapes of soil map units of Lower Diyala project. Journal of College of Education for Women 13, (2) :63-79. https://doi.org/10.5281/zenodo.11391234

2. Al-Jubouri A. M, S. M. Hishem, A. A. Suliman, S. A. El-Desouki, 2023. Survey and Classification of Soil Sheikh Saad sub-District in Wasit Governorate in Iraq using Aerial Photographs by (Drones). In IOP Conference Series: Earth and Environmental Science (Vol. 1252, No. 1, p. 012056). IOP Publishing. doi:10.1088/1755-1315/1252/1/012056

3. Al-Shubaily, I. I. and K. A. Wheib, 2022. Delineation of soil map units using remote sensing and green cover analysis. International Journal of Agricultural & Statistical Sciences, 18. DOI: https://connectjournals.com/ 03899.2022.18.1043

4. An, K., G. D. Xie, Y. F. Leng. and Y. Xiao, 2003. Design of farmland GIS for precision agriculture. Chinese geographical science, 13, 20-24. https://doi.org/10.1007/s11769-003-0079-3

5. Ayamga, M., S. Akaba, and A. A. Nyaaba, 2021. Multifaceted applicability of drones: A review. Technological Forecasting and Social Change, 167, 1-5. https://doi.org/10.1016/j.techfore.2021.120677

6. Bendig, J., K. Yu, H. Aasen, A. Bolten, S. Bennertz, J. Broscheit, M.L. Gnyp, and G. Bareth, 2015. Combining UAV-based plant height from crop surface models, visible, and near infrared vegetation indices for biomass monitoring in barley. International Journal of Applied Earth Observation and Geoinformation, 39, 79-87. https://doi.org/10.1016/j.jag.2015.02.012

7. Bhaskar, B. P., 2018. Pedogeomorphic Analysis in Land Resource Inventory: A Case Study from Central India. Geospatial Technologies in Land Resources Mapping, Monitoring and Management, 273-296. DOI: 10.1007/978-3-319-78711-4_14

8. Buol, S. W., R. J. Southard, R. C. Graham, and P. A. McDaniel, 2011. Soil genesis and classification. John Wiley & Sons. DOI:10.1002/9780470960622

9. Campbell, J. B., 1983. Mapping the Land: Aerial Imagery for Land Use Information. Resource Publications in Geography. Association of American Geographers, 1710 Sixteenth Street, NW, Washington, DC 20009. https://doi.org/10.1080/01431168508948455

10. Esri. 2020. ArcGIS Desktop: Release 10.8, volume 10 Posted: 2020. DOI: dc4691a3990643ccbbfd41e99a9a76fe

11. Gitelson, A. A., Y. J. Kaufman, R. Stark, and D. Rundquist, 2002. Novel algorithms for remote estimation of vegetation fraction.

Remote sensing of Environment, 80(1), 76-87. https://doi.org/10.1016/S0034-4257(01)00289-9

12. Hamad, W. J. and A. A. Suliman, 2021. Use of aerial images taken by drones for survey of soils of Akrkof area located North West of Baghdad in Iraq. Plant Archives 21 ((Suppliment-1)), 1388-1394. https://doi.org/10.51470/PLANTARCHIVES.2021.v21.S1.217

13. Janus, J. and E. Ertunç, 2022. Towards a full automation of land consolidation projects: Fast land partitioning algorithm using the land value map. Land Use Policy, 120, 106282-106288. https://doi.org/10.1016/j.landusepol.2022.106282

14. Jasim, A., A. Zaeen, L.K. Sharma, S.K. Bali, C. Wang, A .Buzza, and A. Alyokhin, 2020. Predicting phosphorus and potato yield using active and passive sensors. Agriculture, 10 (11), pp.564-588. https://doi.org/10.3390/agriculture10110564

15. Jones, C. B., 2014. Geographical information systems and computer cartography. Routledge. p.1-344. https://doi.org/10.4324/9781315846231

16. Lamichhane, S., L. Kumar, and K. Adhikari, 2021. Updating the national soil map of Nepal through digital soil mapping. Geoderma, *394*, article.115041. https://doi.org/10.1016/j.geoderma.2021.115041

17.Liang, Y., W. Kou, H. Lai, J. Wang, Q. Wang, W. Xu, H. Wang, and N. Lu, 2022. Improved estimation of aboveground biomass in rubber plantations by fusing spectral and textural information from UAV-based RGB imagery. Ecological Indicators, 142, 1-13. Article 109286. https://doi.org/10.1016/j.ecolind.2022.109286

18. Lytos, A., T. Lagkas, P. Sarigiannidis, M. Zervakis, and G. Livanos, 2020. Towards smart farming: Systems, frameworks and exploitation of multiple sources. *Computer Networks*, *172*, 1-14. Article 107147. https://doi.org/10.1016/j.comnet.2020.107147

19. Maddikunta, P.K.R., S. Hakak, M. Alazab, S. Bhattacharya, T.R. Gadekallu, W.Z Khan, and Q.V. Pham, 2021. Unmanned aerial vehicles in smart agriculture: Applications, requirements, and challenges. IEEE Sensors Journal, 21(16),17608-17619. https://doi.org/10.1109/JSEN.2021.3049471

20. Pomerening, J.A., 1969. Working as a Free Lance Soil Surveyor. Soil Survey Horizons, 10(1), 12-17. https://doi.org/10.2136/sh1969.1.0012

21. Prabhakara, K., W. D. Hively, and G. W. McCarty, 2015. Evaluating the relationship between biomass, percent groundcover and remote sensing indices across six winter cover crop fields in Maryland, United States. International journal of applied earth observation and geoinformation, 39, 88-102. https://doi.org/10.1016/j.jag.2015.03.002

22. Reg, A., 2010. Unmanned aircraft systems: UAVS design, development and deployment. Austin Reg. John Wiley and Sons, Ltd. Publication,1-332.

23. Roth, L. and B. Streit, 2018. Predicting cover crop biomass by lightweight UAS-based RGB and NIR photography: an applied photogrammetric approach. Precision Agriculture, 19, 93-114. https://link.springer.com/article/10.1007/s11119-017-9501-1

24. Sheng, J., L. Ma, P.A. Jiang, B. Li, F. Huang, and H. Wu, 2010. Digital soil mapping to enable classification of the salt-affected soils in desert agro-ecological zones. Agricultural Water Management, 97(12), 1944-1951. http://dx.doi.org/10.1016/j.agwat.2009.04.011

25. Tucker, C.J., 1979. Red and photographic infrared linear combinations for monitoring vegetation. Remote sensing of Environment, 8(2), 127-150. https://doi.org/10.1016/0034-4257(79)90013-0

26. Wadod, M. M. and F. G. Mohammed, 2023, Review on Drone application methodologies in agriculture precision. In IOP Conference Series: Earth and Environmental Science (Vol. 1202, No. 1, 1202-1216 article. 012001). IOP Publishing. http://dx.doi.org/10.1088/1755-1315/1202/1/012001

27. Wheib, K. A., R. K. Abdullatiff, , and H. A Abdulrahman, 2019. Spatial distribution of some fertility elements in some northern Iraqi soils using geomatic techniques (remote sensing), Plant Archives, 2019, 19, 1295–1301. https://doi.org/10.5281/zenodo.11391729

28. Wheib, K. A., A. S. Ati, and S. A. ALjabar, 2024. Assessment of Unmanned Aerial Vehicle (UAV) Imagery in Monitoring Wheat Canopy Cover in Diwaniya Governorate/ Iraq. Iraqi Journal of Agricultural Sciences. Press print.

29. Wijayanto, A. K., A. Junaedi, A. A. Sujaswara, , M.B. Khamid, L.B. Prasetyo, C. Hongo, and H. Kuze. 2023. Machine Learning for Precise Rice Variety Classification in Tropical Environments Using UAV-Based Multispectral Sensing. AgriEngineering, 5(4), pp.2000-2019. http://dx.doi.org/10.3390/agriengineering5040123

30. Woebbecke, D.M., G.E. Meyer, K. Von Bargen, and D.A. Mortensen. 1995. Color indices for weed identification under various soil, residue, and lighting conditions. Transactions of the ASAE, 38(1), 259-269. doi: 10.13031/2013.27838

31. Wuepper, D., P. Borrelli, and R. Finger. 2020. Countries and the global rate of soil erosion. Nature sustainability, 3(1), 51-55. https://doi.org/10.1038/s41893-019-0438-4